Article

Priming antibody responses to the fusion peptide in rhesus macaques

Check for updates
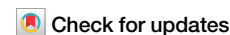
Christopher A. Cottrell [1,2,10], Payal P. Pratap[1,2,10], Kimberly M. Cirelli[2,3], Diane G. Carnathan[2,4], Chiamaka A. Enemuo[4], Aleksandar Antanasijevic [1,2], Gabriel Ozorowski [1,2], Leigh M. Sewall[1,2], Hongmei Gao [5], Joel D. Allen [6], Bartek Nogal[1,2], Murillo Silva[7], Jinal Bhiman[2,8], Matthias Pauthner[2,8], Darrell J. Irvine [2,7], David Montefiori[5], Max Crispin [2,6], Dennis R. Burton [2,8], Guido Silvestri[2,4], Shane Crotty [2,3,9] & Andrew B. Ward [1,2] ✉

Immunodominance of antibodies targeting non-neutralizing epitopes and the high level of somatic hypermutation within germinal centers (GCs) required for most HIV broadly neutralizing antibodies (bnAbs) are major impediments to the development of an effective HIV vaccine. Rational protein vaccine design and non-conventional immunization strategies are potential avenues to overcome these hurdles. Here, we report using implantable osmotic pumps to continuously deliver a series of epitope-targeted immunogens to rhesus macaques over the course of six months to prime and elicit antibody responses against the conserved fusion peptide (FP). GC responses and antibody specificities were tracked longitudinally using lymph node fine-needle aspirates and electron microscopy polyclonal epitope mapping (EMPEM), respectively, to show antibody responses to the FP/N611 glycan hole region were primed, although exhibited limited neutralization breadth. Application of cryoEMPEM delineated key residues for on-target and off-target responses that can drive the next round of structure-based vaccine design.

Most licensed vaccines are delivered via an initial bolus priming immunization followed by subsequent booster immunizations with the same antigen[1]. These booster immunizations are given to increase the titers of neutralizing antibodies and provide an additional opportunity for protection in individuals who did not respond to the priming immunization[1-4]. Conversely, all HIV broadly neutralizing antibodies (bnAbs), which are endowed with the most desirable properties for protection against diverse HIV strains and have demonstrated prophylaxis against infection in recent human trials, develop in response to constant exposure to a continuously evolving antigen, envelope (Env), in the context of long-term infection[5-7]. This continuous stimulation of germinal centers (GCs) drives high amounts of somatic hypermutation required for bnAb evolution[8-14]. We hypothesized that the immune system may therefore be optimized to generate bnAbs in GC responses in the presence of continuous antigen, as is the case

during chronic infection, rather than episodic antigen exposure (e.g. conventional bolus needle immunization). Indeed, short duration (1 to 2 weeks) antigen delivery using subcutaneously (s.c.) implanted osmotic pumps has been used in mice and rhesus macaques (RMs) to protect immunogens from in vivo degradation and facilitate slow release of antigen to stimulate GCs for enhanced germinal center B (B_{GC}) cell and T follicular helper (Tfh) cell responses[15-18]. In all cases, animals immunized via osmotic pump had better overall immune responses compared to control animals receiving bolus immunizations[15-18].

Multiple sites of vulnerability have been identified on the Env glycoprotein against isolated bnAbs, including the CD4 binding site (CD4bs), the V2-apex, the V3-glycan site, the membrane proximal external region (MPER), the gp120/gp41 interface and the fusion peptide (FP)[9,11-13,19-22]. The highly conserved FP is necessary for viral fusion into host cells and has been

[1]Department of Integrative Structural and Computational Biology, The Scripps Research Institute, La Jolla, CA 92037, USA. [2]Center for HIV/AIDS Vaccine Development (CHAVD), The Scripps Research Institute, La Jolla, CA 92037, USA. [3]La Jolla Institute for Immunology, La Jolla, CA 92037, USA. [4]Division of Microbiology and Immunology, Emory National Primate Research Center, Emory University, Atlanta, GA 30329, USA. [5]Duke Human Vaccine Institute and Department of Surgery, Duke University Medical Center Durham, Durham, NC, USA. [6]School of Biological Sciences, University of Southampton, Southampton SO17 1BJ, UK. [7]Koch Institute for Integrative Cancer Research, Massachusetts Institute of Technology, Cambridge, MA 02139, USA. [8]Department of Immunology and Microbiology, The Scripps Research Institute, La Jolla, CA, USA. [9]Division of Infectious Disease and Global Public Health, Department of Medicine, University of California, San Diego, La Jolla, CA, USA. [10]These authors contributed equally: Christopher A. Cottrell, Payal P. Pratap. ✉e-mail: andrew@scripps.edu

utmb Health
Sealy Institute for Vaccine Sciences

shown to be a broadly reactive site of vulnerability on Env in HIV vaccine efforts[23–25]. Previous work in RMs has shown that recombinant BG505 SOSIP Env trimers are capable of eliciting autologous, and in some cases weakly heterologous, neutralizing antibodies directed to the FP epitope[26–28]. Prime-boost regimes employing FP scaffold immunogens and the BG505 SOSIP trimer also have elicited FP-directed neutralizing antibodies in multiple animals, including some with neutralization breadth[29,30]. While this approach shows promise, inducing consistent responses with fewer immunizations will be necessary for an effective vaccine.

Here, we combined a BG505-based immunogen series engineered to prime antibody responses to the FP epitope with a platform for continuous immunogen delivery over the course of six months in non-human primates (NHPs). Further, we sought to recapitulate some aspects of the immune response during chronic infections by varying immunogen over the course of the continuous delivery with assorted glycan presence around the FP. Using electron microscopy polyclonal epitope mapping (EMPEM), we carefully monitored the antibody responses over time to evaluate our strategy.

Results

Design of a fusion peptide epitope targeting immunogen

The stabilized BG505 SOSIP.v5.2 was used as the basis for engineering a series of trimer immunogens designed to prime and focus antibody response to the FP epitope[31]. For the priming immunogen, we removed the N611 glycan to make the FP epitope more accessible to B cell receptors (BCRs) and added a potential N-linked glycosylation site (PNGS) at N289 to reduce off-target antibody responses directed to the N289 glycan hole (Fig. 1a)[32–34]. In the Boost#1 immunogen we added a PNGS at N241 to restrict the angles of approach for BCRs to target the FP epitope in a bnAb-like fashion (Fig. 1a). Subsequently, the Boost#2 immunogen was designed to restore the N611 PNGS with an additional S613T mutation that enhances glycan occupancy at the N611 site (Fig. 1a)[35]. The BG505 Env sequence has several residues surrounding the FP epitope that are poorly conserved when compared to the Los Alamos National Library (LANL) HIV Sequence database (https://www.hiv.lanl.gov/content/sequence/HIV/HIVTools.html); particularly, H85 (8.6% prevalence among global strains) and K229 (13.0% prevalence), which have been shown to play a role in the epitopes of autologous nAbs elicited by BG505 SOSIP in rabbits and RMs[26,36]. Hence, for the Boost#3 immunogen, we mutated H85 and K229 to the consensus residues valine (39.0% prevalence) and asparagine (78.6% prevalence), respectively (Fig. 1a). The antigenicity of all four immunogens was evaluated by biolayer interferometry using a panel of anti-HIV Env antibodies (Fig. 1a and Supplementary Fig. 1). All four immunogens bound well to the quaternary specific bnAb PGT145 and showed little binding to the gp120 (monomer)-specific F105 antibody (Fig. 1b)[37–39]. All four immunogens showed low binding to the V3 targeting non-nAbs 19b and 14e, no detectable binding to a panel of non-nAbs including those targeting the gp41 post-fusion conformation (F240, 7B2, and 98-6), and high binding to the BG505-SOSIP elicited base-binding mAb RM19R (Supplementary Fig. 1)[26]. Additionally, all four immunogens bound to known FP targeting bnAbs (PGT151, VRC34, and ACS202) (Fig. 1b)[23,25,40]. The Prime immunogen bound to an inferred germline (iGL) version of FP-targeting RM20F, originally isolated from an NHP immunized with BG505 SOSIP (Fig. 1b)[26]. The iGL-RM20F mAb bound weakly to the Boost#1 immunogen and did not bind to the Boost#2 or Boost#3 immunogens (Fig. 1b). The mature version of RM20F, which can potently neutralize autologous virus, also exhibited diminished binding to the later boost immunogens (Fig. 1b)[26]. Hence, the Prime and Boost#1 immunogens were designed to engage a known FP BCR while the Boost#2 and #3 were designed to mature toward breadth and away from the strain-specific phenotype embodied by RM20F.

Two groups of six RMs each were immunized continuously over the course of 24 weeks using s.c. implanted osmotic pumps (Fig. 1c). The pumps were filled with immunogen adjuvanted with Matrix-M (which has been successfully incorporated in the approved Novavax protein subunit COVID vaccine[41]) and implanted bilaterally in the left and right thighs, with

exchanges occurring every 4 weeks[42]. The experimental group received the Prime immunogen in the first two pumps, the Boost#1 immunogen in the 3rd pump, the Boost#2 immunogen in the 4th pumps and Boost#3 in the final two pumps (Fig. 1c). The control group received the Boost#2 immunogen in all six pumps (Fig. 1c). At the conclusion of the continuous immunogen delivery portion of the study, the animals were given a s.c. bolus immunization with an octameric nanoparticle immunogen displaying 8 copies of either the Boost#3 or Boost#2 immunogens for the experimental and controls groups, respectively, with the FP still accessible (Supplementary Fig. 2a). Multimeric display scaffold immunogens are thought to be able to induce memory B cells (MBCs) to become plasma cells similar to intact whole-virus re-exposure[43] as nanoparticles are also able to cross-link BCRs of MBCs due to their high avidity[44]. The nanoparticle immunization was given bilaterally in the left and right thighs with the 3M-052 stable emulsion (SE) adjuvant[45]. The animals were boosted again at week 40 via s.c. bolus immunization using SMNP adjuvant with either the Boost#3 or Boost#2 soluble trimer immunogens for the experimental and control groups, respectively (Fig. 1c) as a contemporaneous study revealed SMNP to be a highly potent and superior adjuvant[46].

GC responses were durable over the course of six months continuous immunization

To monitor the GC responses during continuous immunogen delivery, longitudinal lymph node (LN) fine needle aspirates (FNAs) were used to sample the draining inguinal LNs throughout the study (Fig. 1c). Previous work has shown that LN FNAs are well tolerated and represent the cellular composition of the whole LN[15,47]. B_{GC} cell frequencies rose during the course of the first pump and remained elevated throughout the study (Fig. 2a, b). Cells taken from the LN FNAs were stained with fluorescent probes of the Prime and Boost#2 immunogens. Overall, the frequency of B_{GC} cells that were double positive for both immunogens was consistent between groups throughout the study (Fig. 2c–f). The frequency of B_{GC} cells that were positive for only the Prime immunogen was significantly greater in the experimental group, consistent with a bias toward the gp41-N611/FP region. (Fig. 2e–h).

Longitudinal monitoring of humoral immune responses revealed early targeting of the FP epitope in the experimental group

To assess antibody specificities elicited by immunization, polyclonal IgG isolated from plasma blood draws was digested into fragments antigen binding (Fabs) and subjected to EMPEM analysis[48]. Prior to week 18, EMPEM analysis was conducted using either the Prime (expt group) or Boost #2 (ctrl group) immunogens and probes, and the results are reported as composites of both runs. Polyclonal Fabs isolated as early as week 6 from the experimental group targeted the gp41-N611/FP region (Fig. 3). In both immunization groups, antibodies directed to the base of the trimer were observed as early as week 6 and persisted throughout the duration of the study (Figs. 3c, d), consistent with immunodominance of the base epitope[16,26,49,50]. Antibody responses directed to non-FP, non-neutralizing epitopes other than the base of the trimer (V5/C3, V1/V3, gp120/gp120 interface (IF), and N355/N289 glycan hole epitope) were observed earlier and more consistently in the control group during the continuous immunogen delivery phase of the study (Fig. 3c). By week 14 (2 weeks into the pump containing the Boost#2 immunogen), antibody responses directed towards these off-target epitopes became prevalent in the experimental group (Fig. 1c). This delay in eliciting antibodies directed to off-target epitopes other than the base of the trimer in the experimental group suggests the gp41-N611/FP region may have been preferentially targeted relative to the others. By the end of the continuous immunogen delivery phase both groups of animals had a similar prevalence of antibodies directed to off-target epitopes with the experimental group also maintaining a high prevalence of gp41-N611/FP region directed antibodies (Fig. 3c).

The bolus immunizations with the octameric immunogen did not boost the BG505 Env binding titers in either group (Fig. 3a) nor did they
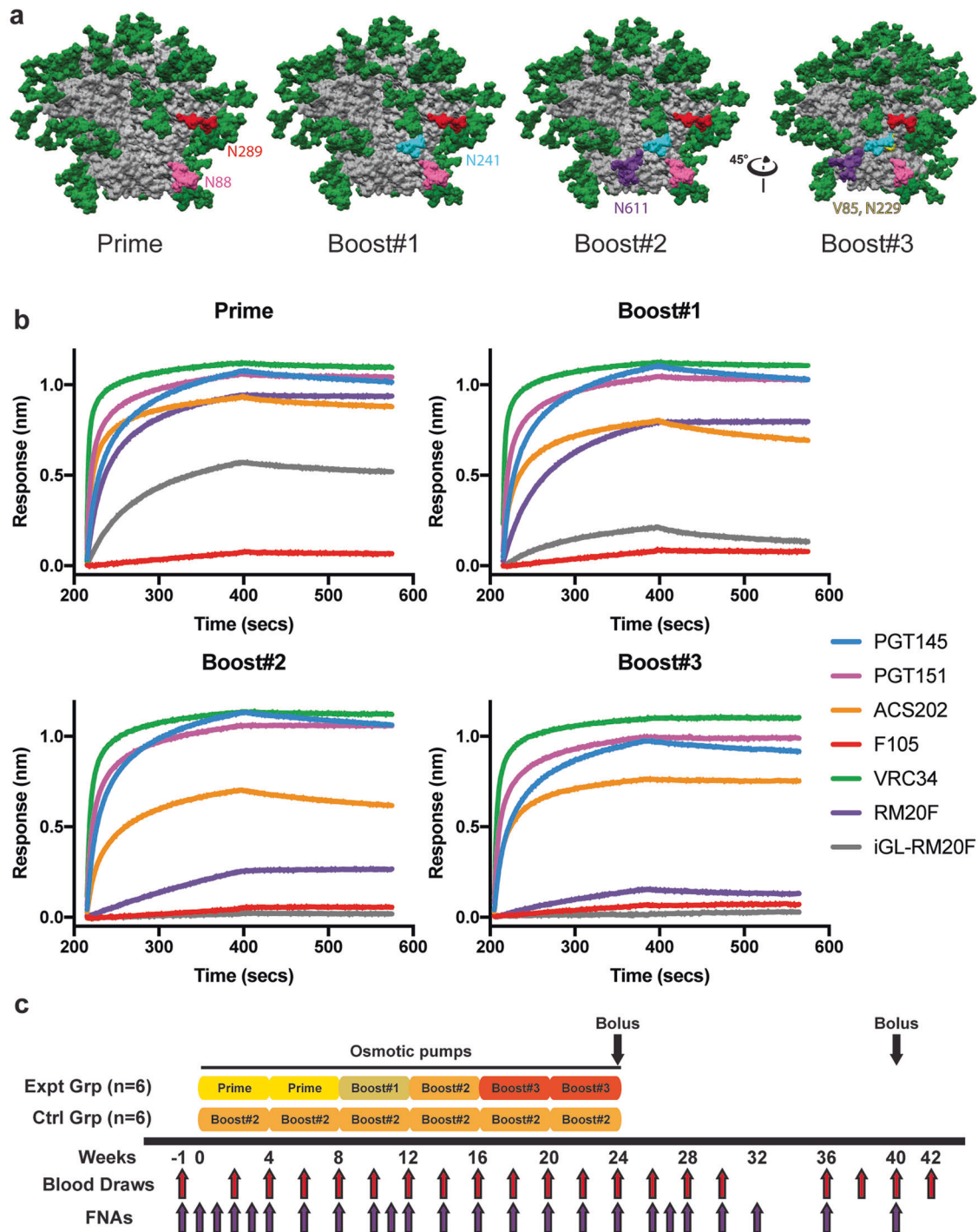
Fig. 1 | FP focused immunogen design and immunization scheme. a Surface representations of the BG505 SOSIP.v5.2 immunogen with mutations designed to focus antibody responses to the FP epitope. N88 glycan in pink. N611 glycan in purple. Introduced N289 glycan in red. Introduced N241 glycan in turquoise. Consensus mutations around the FP epitope shown in yellow. **b** Antigenicity was assessed using BLI on panel of anti-Env mAbs: PGT145 (apex), PGT151 (FP), ACS202 (FP), VRC34 (FP), RM20F (FP), iGL-RM20F (FP), and F105 (anti-gp120, non-Nab). **c** Immunization scheme.

have a detectable impact on the epitopes visualized by EMPEM analysis (Fig. 3d). Instead, the octameric immunogen appeared to have induced a de novo antibody response directed to the protein core of the nanoparticle (Fig. S2b). Compared to the end of the continuous pump and octameric immunogen bolus immunizations, week 40 bolus immunizations with trimer immunogen and SMNP led to a bigger increase of BG505 binding titers in the experimental group compared to the control groups (Fig. 3a) with no detectable impact on the epitope diversity seen in the EMPEM analysis in either group (Fig. 3d). Overall, FP recognizing antibody evolution was

moderate during the osmotic pump portion of the study, with a slight increase after the trimer + SMNP bolus immunization (Fig. 3e)

At the end of the continuous immunogen delivery phase, the BG505 autologous neutralization titers were lower in the experimental groups compared to the control group (Fig. 4a). The control group neutralization titers were similar to titers from other soluble trimer immunizations in NHPs via osmotic pump[15,17]. The bolus immunization with the octameric immunogen did not improve the BG505 autologous neutralization titer for either group (Fig. 4b, Supplementary Table 1). Sera from animals in the
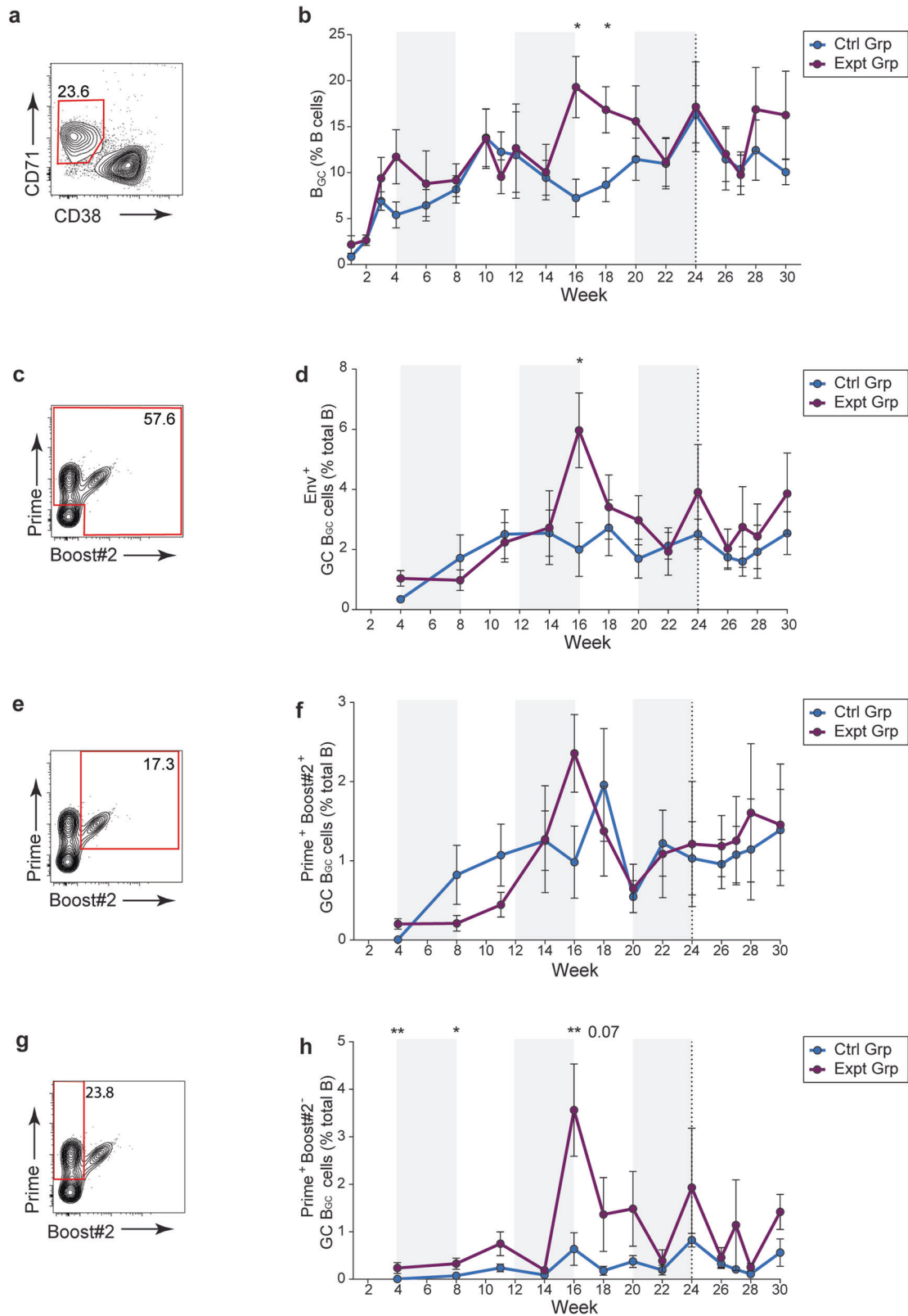
Fig. 2 | Sustained delivery immunization results in enduring GC responses.
a Representative GC B cell flow cytometry. **b** Quantification of B_{GC} cell kinetics as a percentage of total CD20$^+$ B cells. **c** Representative total Env trimer-specific binding flow cytometry, gated on B_{GC}B cells. **d** Quantification of total Env trimer-specific B_{GC} cells kinetics as a percentage of total CD20$^+$ B cells. **e** Representative Prime and Boost#2 dual-specific binding flow cytometry, gated on B_{GC} cells. **f** Quantification of Prime and Boost#2-specific cell kinetics as a percentage of total CD20$^+$ B cells. **g** Representative Prime immunogen-specific flow cytometry, gated on B_{GC} cells. **h** Quantification of Prime immunogen-specific B_{GC} cell kinetics as a percentage of total CD20$^+$ B cells. Plot shows the mean of left and right side FNAs (analyzed separately) with standard error of means (SEM), $*p \leq 0.05$, $**p \leq 0.01$.
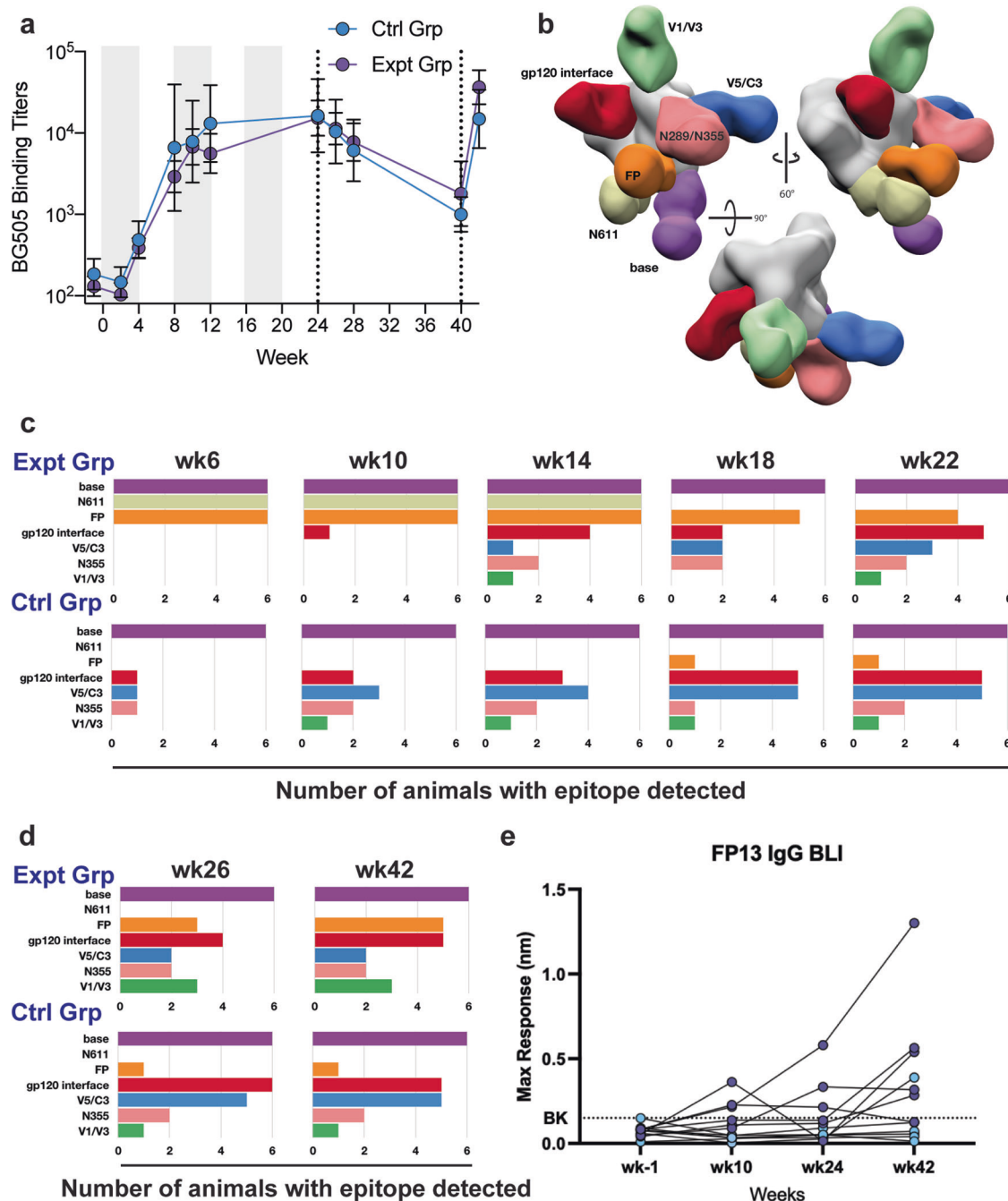
Fig. 3 | Longitudinal monitoring of the humoral immune response by ELISA, BLI and negative stain EMPEM. a Plasma IgG binding ELISA of each group over the duration of the study. Six animals per group, showing geometric mean titers ± geometric SD. **b** Composite 3D map representing the epitopes observed in the longitudinal negative stain EMPEM analysis. **c** Longitudinal negative stain EMPEM analysis of the continuous immunogen delivery phase of the study. Bar graphs show how many animals per group made antibodies directed to each specific epitope. Colored to match (**b**). **d** Longitudinal negative stain EMPEM analysis 2 weeks after each bolus immunization, colored to match (**b**). **e** Plasma IgG binding of FP13 linear peptide BLI at weeks -1 (baseline), 10 (2 weeks post Boost #1), 24 (end of pump portion of the study), and 42 (2 weeks post final bolus immunization) for the control group (blue circles) and experimental group (purple circles).

experimental group potently neutralized the BG505 pseudovirus with the N611 glycan knocked out (N611A) (Fig. 4C, Supplementary Table 1). This enhancement in neutralization activity following the removal of the N611 glycan was absent in the control group (Fig. 4c, Supplementary Table 1). Adding a glycan to the V5 loop (T465N) decreased the neutralization activity of the sera from the control group (Fig. 4d, Supplementary Table 1), consistent with the V5 epitope seen in the EMPEM analysis which was likely responsible for the autologous neutralization activity. Additionally, lengthening the V1 by two amino acids (133aN and 136aA), which has been previously shown to be part of a neutralization epitope targeted in BG505

SOSIP animals, decreased the neutralization activity of sera from animals 31943 (Ctrl Grp) and 32607 (Expt Grp), both of which had V1 epitope targeting antibodies detected by EMPEM analysis (Fig. 3b–d)[27,51,52]. Neither group demonstrated significant neutralization breadth when assessed on the global panel or an FP-sensitive panel of pseudoviruses (Supplementary Tables 2, 3)[30,53]. BG505 neutralization titers significantly increased after trimer and SMNP bolus immunizations (week 42) compared to after octameric bolus immunizations (week 26) (Fig. 4f and Supplementary Table 1). Week 42 FP-sensitive neutralization titers showed two of the animals in the experimental group were able to weakly neutralize three out of nine
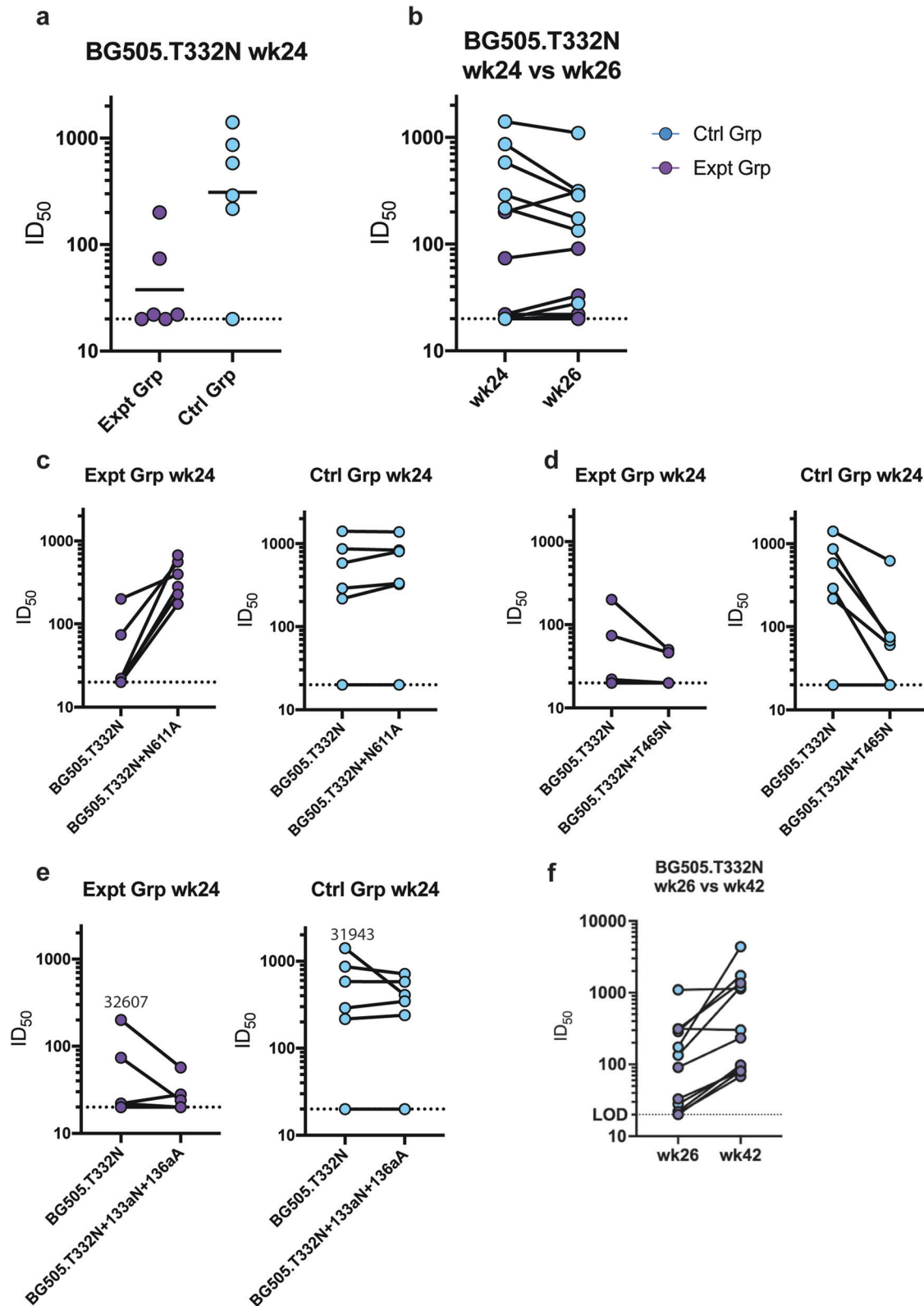
Fig. 4 | Serum neutralization activity. a Week 24 serum neutralization activity against the BG505.T332N pseudovirus. Dotted lines indicate detection limit for the assay. **b** Comparison of BG505.T332N pseudovirus neutralization activity against before (week 24) and after (week 26) bolus nanoparticle immunization. Connecting lines indicate specific animal response differences seen between the two time points. **c** Week 24 serum neutralization activity against the BG505.T332N + N611A pseudovirus. **d** Week 24 serum neutralization activity against the BG505.T332N + T465N pseudovirus. **e** Week 24 serum neutralization activity against the BG505.T332N + 133aN_136aA pseudovirus. **f** Week 26 versus week 42 serum neutralization activity against BG505.T332N pseudovirus.

pseudoviruses in the FP sensitive panel while none of the animals in the control group were able to neutralize any of the pseudoviruses in the FP-sensitive panel at this time point (Supplementary Table 2). Further, in-depth epitope mapping analysis was done on the animal with higher neutralization titers, which is discussed later.

At the week 18 time point, we transitioned to using only the Boost#2 immunogen as a probe for both groups. This was done to detect FP directed antibodies that could accommodate the N611 and N241 glycans present in the Boost#2 immunogen. As expected, the use of this trimer resulted in the inability to detect N611 glycan hole-directed antibody responses in the experimental group after week 18 (Fig. 3c, d).

Surprisingly, several animals in both groups made antibody responses directed to the N355/N289 glycan hole epitope, despite the introduction of the N289 PNGS sequon in all the immunogens used (Fig. 3c, d). Post-hoc, site-specific glycan occupancy analysis was conducted on the immunogens (Supplementary Figs. 3–7). Unfortunately, the analysis could not detect peptides corresponding to the N289 site and glycan occupancy at that site could not be measured. Given the heterogenous occupancy of the introduced N241 PNGS in the Boost#1, Boost#2 and Boost#3 immunogens, along with the EMPEM data, the N289 glycan occupancy was likely less than 100% in the immunogens and flow cytometry probes.

CryoEM elucidation of epitope/paratope interfaces of polyclonal Fabs elicited through immunization against the Boost#2 Immunogen

Fusion Peptide. CryoEMPEM (EMPEM using vitrified instead of negatively-stained samples) can resolve different classes of antibodies with overlapping binding sites within one sample and provide a more detailed picture of epitope/paratope interfaces compared to negative stain (ns) EMPEM[49]. The nsEM analysis of animal Rh.32613-week 42 protein complex revealed interesting FP-directed responses and was chosen for cryoEM analysis. 13 distinct, high resolution (≤4.5 Å) antibody-immunogen maps were reconstructed from this single dataset, including four different antibodies against the FP region (FP1-4) (Supplementary Fig. 5). Of the four maps, FP1 and FP3 had the most interpretable density such that atomic modeling could be attempted.

The FP3 map (~3.5 Å resolution) contains a fully resolved N-terminus of the FP, which, due to the inherent flexibility of the hydrophobic linear peptide, is typically resolved only via cryoEM when stabilized by an anti-FP antibody as seen in FP3 and bnAbs isolated from humans (Fig. 5a, b)[23,25,30,54–56]. In the FP3 complex conformation, the FP N-terminus is stabilized via interactions with L645 (90.2% prevalence) and E648 (58.6% prevalence) of the adjacent gp41 subunit and residue 69 of the light chain framework region 3 (LFR3) (Fig. 5c, d). Atomic modeling of the FP3 antibody backbone revealed a long heavy chain complementarity determining region 3 (HCDR3) with a predicted length of 25 amino acids (aa), which is a common feature of bnAbs (Supplementary Fig. 5a and Table 1)[13,57]. The densities of the HCDR3 side chains suggest the presence of at least three aromatic residues and other medium-sized hydrophobic residues interacting with the FP (Fig. 5d)[58]. A hydrophobic pocket forms around a predicted aromatic residue at position 102 of the heavy chain, presumed to be a tryptophan based on the density, which interacts with the I515 (53.0% prevalence) and V518 (43.2% prevalence) residues of the FP as well as I641 (19.4% prevalence) on the heptad repeat domain 2 (HR2) of gp41. Another hydrophobic pocket is found around F522 of the FP, which is further stabilized by the presence of two aromatic residues at positions 108 and 109 of the HCDR3 (Fig. 5d). The long HCDR3 also interacts with many residues of the C1 region of gp120, including highly conserved residues T77 (98% prevalence), D78 (98.7% prevalence), Q82 (prevalence 94.0%), E83 (99.5% prevalence) as well as less conserved residues I84 (45.2%), H85 (8.6%) and E87 (56.1%).

There are 4 canonical glycans around the FP at positions N88, N230, N241 and N611, some of which have been shown to be important for FP bnAb binding and affinity such as glycans at N88 and N241 for VRC34 and ACS202, respectively[23,25,30,55]. Wild type BG505 does not contain either N230

or N241 glycan sites, although the N241 glycan site was knocked-in for the boosting immunogens in this study. In the case of FP3, interactions were observed between N88 glycan and residues 76 and 77 of HFR3. On the adjacent gp41 of the stabilized FP, HFR3 residue 68 is predicted to interact with the N611 glycan and the T613 residue. While not a canonical FP glycan, the glycan at N637 on the adjacent gp41 also interacts with LCDR2. Using the Ward Lab rhesus macaque germline database (RhGLDb), we predicted the V_H of FP3 to be IGHV4-AFI*01, with up to four amino acid differences between our model and the germline genes (~96% sequence identity), possibly due to SHM.

FP1 (~3.7 Å resolution) resembles RM20F in its angle of approach, with only a partially resolved FP starting at position G516, engagement with the N88 glycan, and contacts with the poorly conserved residues H85 and K229 in the C1 and C2 regions of gp120, respectively[26] (Fig. 6). Atomic modeling predicts that FP1 HCDR3 is approximately 18 residues long, two less than the HCDR3 for RM20F (Fig. 6b and Table 1). The predicted V_H of FP1 using the RhGLDb is LJI.Rh_IGHV3.76.a_S4190 with up to 5 aa differences between the modeled sequence and this V_H. RM20F, on the other hand, is predicted to use IGHV3-AFY*10 as its V_H, indicating only 85.6% sequence similarity by amino acid (88.1% nucleotide) between the two predicted V_H.

Although FP1 and RM20F share a high percentage of similarity in V_H gene usage as well as angle of approach, RM20F potently neutralized BG505.T332N pseudovirus[26] whereas animal Rh.32613 serum was only weakly neutralized BG505.T332N (Supplementary Table 2). As mentioned earlier, wildtype BG505 Env isolates do not have glycans at positions 230 (35% global prevalence of a PNGS) and 241 (97% global prevalence of PNGS) of gp120. The RM20F lineage evolved in a macaque after multiple rounds of immunization with BG505 SOSIP.664, a soluble, truncated trimer with glycan holes at positions 230, 241 and 289, mimicking the native BG505 Env glycoprotein ectodomain. In this study, FP1 evolved in the presence of a glycan at position 241 as early as 8 weeks after the study began, unlike RM20F, which was isolated after more than 20 weeks of repeated immunizations of BG505 SOSIP.664[26]. Structural analysis of RM20F and FP1 revealed the impact of the N241 glycan presence in light chain interaction for the antibodies.

In RM20F, the aspartic acid at the N-terminus of the light chain creates a salt bridge with lysine at position 231 of the C2 region (Fig. 6d). When the 241 glycan is present, this interaction would not be possible, as the glycan would occlude the required K231 conformation, and neutralization potency of RM20F decreases more than 6-fold[26]. FP1 light chain N-terminus does not coordinate with K231, as this antibody has evolved to accommodate the N241 glycan instead. This could be a contributing factor to why Rh.32613 serum indicated weak BG505 SOSIP.664 neutralization, unlike RM20F, even though the two antibodies share similar angles of approach and heavy chain sequence identity.

Off-Target Responses. An additional four maps were also reconstructed for polyclonal responses against the gp41 base (Base1-4) (Supplementary Fig. 4). Base-4 is the best resolved and demonstrates that residues R500 of gp120 and W623 of the intraprotomeric gp41 are important for this interaction. The predicted heavy chain for the pAb contains an HCDR3 that reaches into the base of the trimer and nestles between the R500 and W623 residues (Supplementary Fig. 6a)[59,60]. Analysis of pAbs elicited against BG505 SOSIP base in other NHP studies also showed the prevalence of these residues within the base epitope/paratope interface[49]. The global prevalence of an arginine at position 500 on HIV Env is 24.8% but the prevalence of a positively charged residue (R, K, or H) at this position is 75.5%. The tryptophan clasp of gp41 (W623, W628 and W631) is critical for maintaining the prefusion confirmation of Env before protein rearrangement for viral entry upon engagement of the FP[59,60]. As a result, W623 is 99.5% conserved according to the LANL HIV Database. Two maps were derived that contained antibody responses to the gp120/gp120 IF epitope (Supplementary Fig. 4), IF-1 and IF-3, each with sufficient resolution to explore the epitope/paratope interface. IF-1 Ab interacts with residues of the V3 loop including the
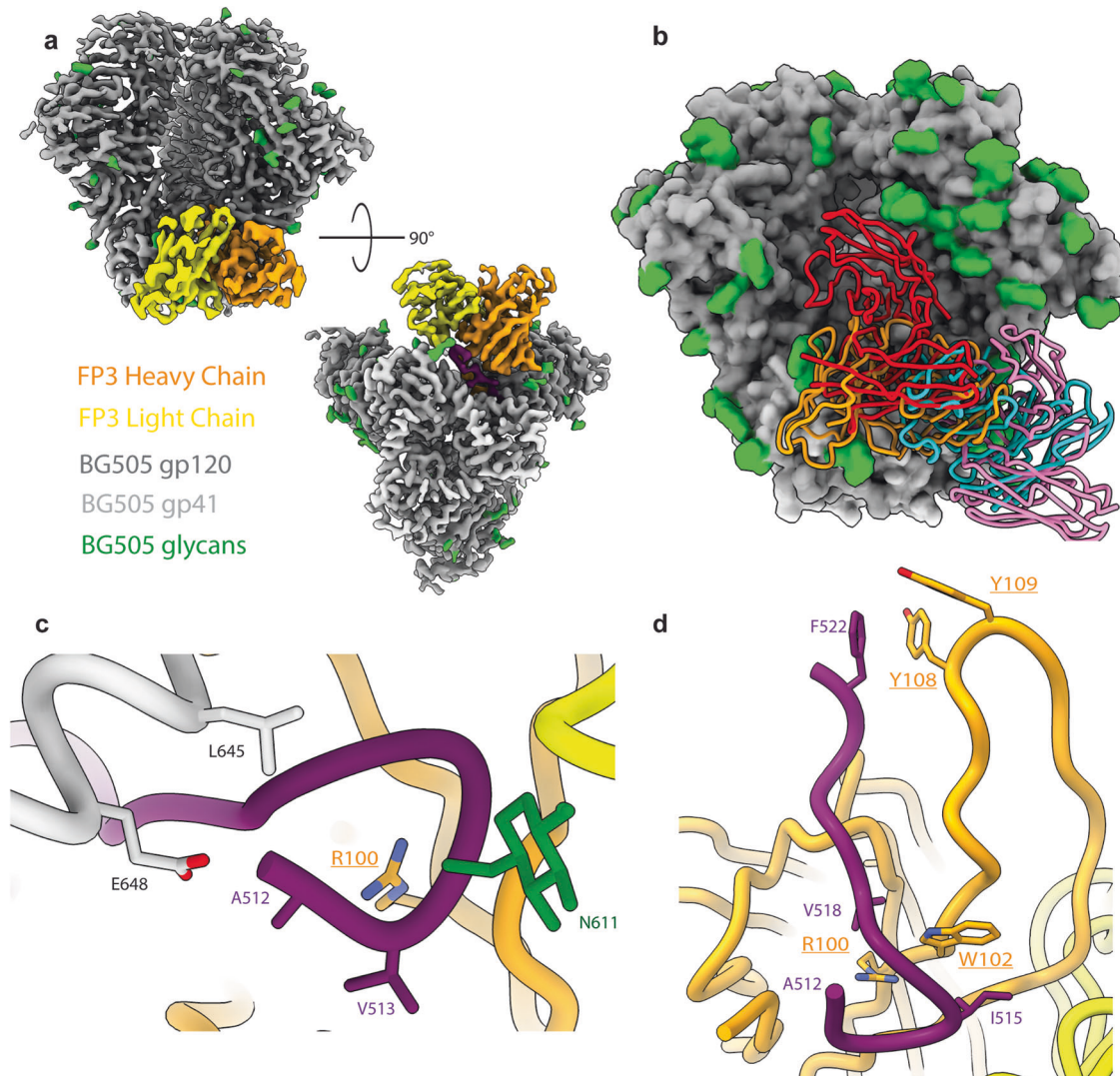
Fig. 5 | CryoEM Analysis of FP3. a Boost #2 in complex with the predicted heavy chain (orange) and light chain (yellow) of FP3 antibody targets the FP epitope area. **b** Alignment of FP3 (orange) compared to known human bnAbs PGT151 (red), VRC34.01 (cyan), and ACS202 (pink). **c** FP is fully resolved in FP3 due to stabilization of the N-terminus by the antibody (underlined residues are inferred from density; residues not underlined are sequence verified). **d** The HCDR3 of FP3 antibody interacts with FP by creating hydrophobic pockets around the N-terminus as well as around F522 with the presence of hydrophobic aromatic residues.

stabilizing mutation A316W that was introduced beginning in SOSIP.v4 constructs to limit recognition by weakly/non-neutralizing antibodies (Supplementary Fig. 6b)[31,61]. Antibody responses against this epitope have been reported in other NHP studies[49]. While the V3 loop and W316 residue are also in the epitope interface for IF-3 map, the antibody has additional interactions charged residues in the C1 and C2 regions including K65 (6.7% prevalence), H66 (99.9% prevalence) and K207 (99.3% prevalence) (Supplementary Fig. 6c). Although we had introduced a glycan into position 289, which has a global prevalence of 70.0% for a PNGS at this position but is not present in wild type BG505, antibody responses were observed against the N289 residue, indicating the absence of the glycan at this position (Supplementary Figs. 4 and 6c), opening this region for immune recognition.

Discussion

Here we demonstrate that immunogen design was an effective means to successfully prime FP-directed antibody responses as well as the adjacent N611 glycan hole epitope. Over time however, and consistent with previous NHP slow delivery immunization studies, we observed a wide variety of epitopes targeted in this immunization protocol[15,28]. Despite introducing the

N289 PNGS, typically missing in wild type BG505, into all the immunogens used in this study, several animals in both groups elicited antibodies against the N355/N289-glycan hole epitope. Glycan analysis was thus conducted on the immunogens to discern site specific glycan occupancy (Supplementary Figs. 7–10). The analysis was not able to detect glycan occupancy at N289 site, but previous studies have shown that recombinant protein expression of Env trimer can have glycan under occupancy, even at highly conserved glycan sites[49]. For example, the introduced N241 PNGS in Boost#1, Boost#2 and Boost#3 immunogens showed differential levels of occupancy, so heterogenous occupancy for the N289 glycan would not be surprising and would explain the antibody evolution against this site. CryoEM analysis of this epitope/paratope interface confirmed a lack of density corresponding to the N289 glycan, consistent with glycan under occupancy at this residue.

Presence of the V5/C3 epitope in EMPEM correlated with autologous neutralization activity that was subsequently reduced or eliminated by introducing a PNGS into the V5 loop at position 465[27,52]. The gp120/gp120-interface antibodies were not seen in previous EMPEM analysis in animals immunized with BG505 SOSIP.664, and based on previous results in RMs[26,30,49], are thought to result from the A316W stabilizing mutation that

Table 1 | Fusion peptide nAbs

FP Abs (PDB Code)	Species	Antigen Genotype	FP aa contacts	Non-FP aa contacts	Glycan contacts	VH Gene	HCDR3 length (aa)
VRC34.01 (5I8H)	Human	BG505	512-520	D80, E83-H85, E87, K229- K231, S241	N88	IGHV1-2*02	13
(6NC3)		AMC011	512-520	E83-V85	N88, N241		
PGT151 (6OLP)	Human	AMC011	512-522	A58, P79, N80 Q82-V84, T244- Q246 V539 R542-L543, Y638 S640, L641 Y643, T644 E647	N88 N611, N637	IGHV3-30*04	28
ACS202 (6NC2)	Human	AMC011 v4.2	512-520, A525	V85, E87, S528, A532-A533, M535 T536	N88, N241	IGHV3-30*03	24
RM20F (6VN0)	Macaque	BG505	518, 520-521	P81, E83-H85, E87, K229, K231, M535, T536, V539, R542, Q650	N88	IGHV3- AFY*10	20
FP1 (8SW7)	Macaque	BG505	517-520-522, 524, 525	D78-H85, E87, K229, S528, A532 T536, V539, R542, Q640, G644, E647, E648	N88, N241	LJI.Rh_IGHV3.76.a_S4190	18*
FP3 (8T2E)	Macaque	BG505	512-522	P76-P79, E82-H85, E87, A219-I225, T244-Q246, I491, R542-L544, S546, T613-W614, Y638, Q640-I641, Y643	N88, N637, N611	IGHV4-AFI*01	25*
DF1W-a.01 (6MPH)	Macaque	BG505 DS-SOSIP	512-521	80-85, E87, V539, R542, N543 I641 G644, L645 E648	N88	IGHV4-AFQ*01_S0868	10
A12V163-a.01 (6N1V)	Macaque	BG505 DS-SOSIP	512-521	N80, E83-N88, K229, S528	N88	IGHV4-AFB*01	14
A12V163-b.01 (6MPG)	Macaque	BG505 DS-SOSIP	512-519	D78, N80, Q82, E83, I84, H85, E87,79-85, E87, K229, S241, A524, S528, A532, R542, Q640	N88	IGHV3-ADR*01	11
DFPH-a.15 (6N1W)	Macaque	BG505 DS SOSIP	512-520	N80, P81, Q82, E83, I84, H85, V539, R542, Q640, G644, E647, E648	N88	IGHV4-AGR*01_S4099	19
0PV-b.01 (6OT1)	Macaque	BG505 DS SOSIP	512-520	N80, M535, S613, Q640 G644, E648	N637	IGHV4-AGR*01_S4099	14

Summary of isolated human or NHP nAbs against the FP, including the FP contacts, non-FP contacts, glycan contacts and, VH gene usage and HCDR3 lengths. Contacts are defined as a distance (≤5 Å for mAbs and ≤6 Å for pAbs) between antibody and HIV Env trimer atoms.

falls within that epitope and is present in the BG505 SOSIPv5.2 construct used as the basis for immunogen design in this study.

CryoEMPEM further elucidated the FP and off-target responses. We were able to model two polyclonal antibodies, FP1 and FP3, that were able to either partially or fully stabilize the highly hydrophobic and flexible FP, respectively. FP3, with an estimated 25 aa HCDR3 not only fully engages with the FP but also makes contacts with other interprotomeric gp120 and gp41 regions. FP1, on the other hand, closely resembles RM20F, an antibody isolated from NHPs with autologous neutralization against BG505, in angle of approach, major contact residues and partial engagement with the FP, however light chain usage differences may explain the difference in neutralizing capabilities of RM20F and Rh.32613 serum analysis.

Overall, this study shows that the FP/N611-glycan hole targeting antibodies can be reproducibly primed in RMs using an immune-focusing approach. GC response could be extended using continuous immunogen delivery but no gain in antibody neutralization breadth was observed relative to historical controls with short duration pumps or bolus immunizations. Hence, despite improved epitope-specific responses and highly active and long-lived GCs, the NHPs failed to generate a broadly neutralizing antibody response. We therefore conclude that germline-targeting and additional immunogen design efforts are likely needed to improve the anti-FP antibody response and to elicit antibodies capable of neutralizing viruses with complete N611 glycosylation.

Methods

Rhesus Macaques

Twelve Indian origin rhesus macaques (*Macaca mulatta*) were sourced and housed at the Emory National Primate Research Center and maintained in accordance with NIH guidelines. This study was approved by the Emory University Institutional Animal Care and Use Committee (IACUC) [IACUC# 201700723]. Animal care facilities are accredited by the U.S. Department of Agriculture (USDA) and the Association for Assessment and Accreditation of Laboratory Animal Care (AAALAC) International. When osmotic pumps were implanted, animals were kept in single, protected contact housing. At all other times, animals were kept in paired housing. Animals were treated with anesthesia (ketamine 5-10 mg/kg or telazol 3–6 mg/kg) and analgesics for procedures such as osmotic pump implantation and removal, subcutaneous immunization, blood draws, and lymph node fine needle aspirates as per veterinarian recommendations and IACUC approved protocols. Rhesus macaques were male, an age range of 3-4 years old, and at the start of the study a median weight of 5 kilograms. Animals were grouped to divide age, weight and gender as evenly as possible between the two groups. After completion of the proposed study, animals were transferred to other researchers upon the approval of the veterinarians.

Immunogen and probe generation

The BG505 SOSIP.v5.2 and BG505 SOSIP.v5.2-Avitag plasmids were generously provided by Dr. Marit van Gils[31]. Site-direct mutagenesis (QuikChange Multi kit, Agilent) was used create the plasmids encoding the Prime, Boost#1, Boost#2, Boost#3, Prime-Avitag, and Boost#2-Avitag. Specific mutations relative to BG505 SOSIP.v5.2 are listed in Table S4. Immunogens and Avi-tagged probes were produced in HEK293F cells and purified using PGT145 affinity chromatography followed by size-exclusion chromatography as described previously[61]. The Avi-tagged proteins were biotinylated using the BirA enzyme (Avidity) according to the manufacturer's protocol. The resulting biotinylated proteins are referred to using the descriptor AviB.

Immunizations

Osmotic pumps (Alzet model 2004) were loaded with 50 μg soluble Env trimer immunogen + 75 U Matrix-M adjuvant (Novavax) in PBS according to Fig. 1c. Two pumps were subcutaneously implanted into each animal (one pump each in the left and right mid-thighs). The immunogen/adjuvant mixture was secreted continuously over the course of 4 weeks. The
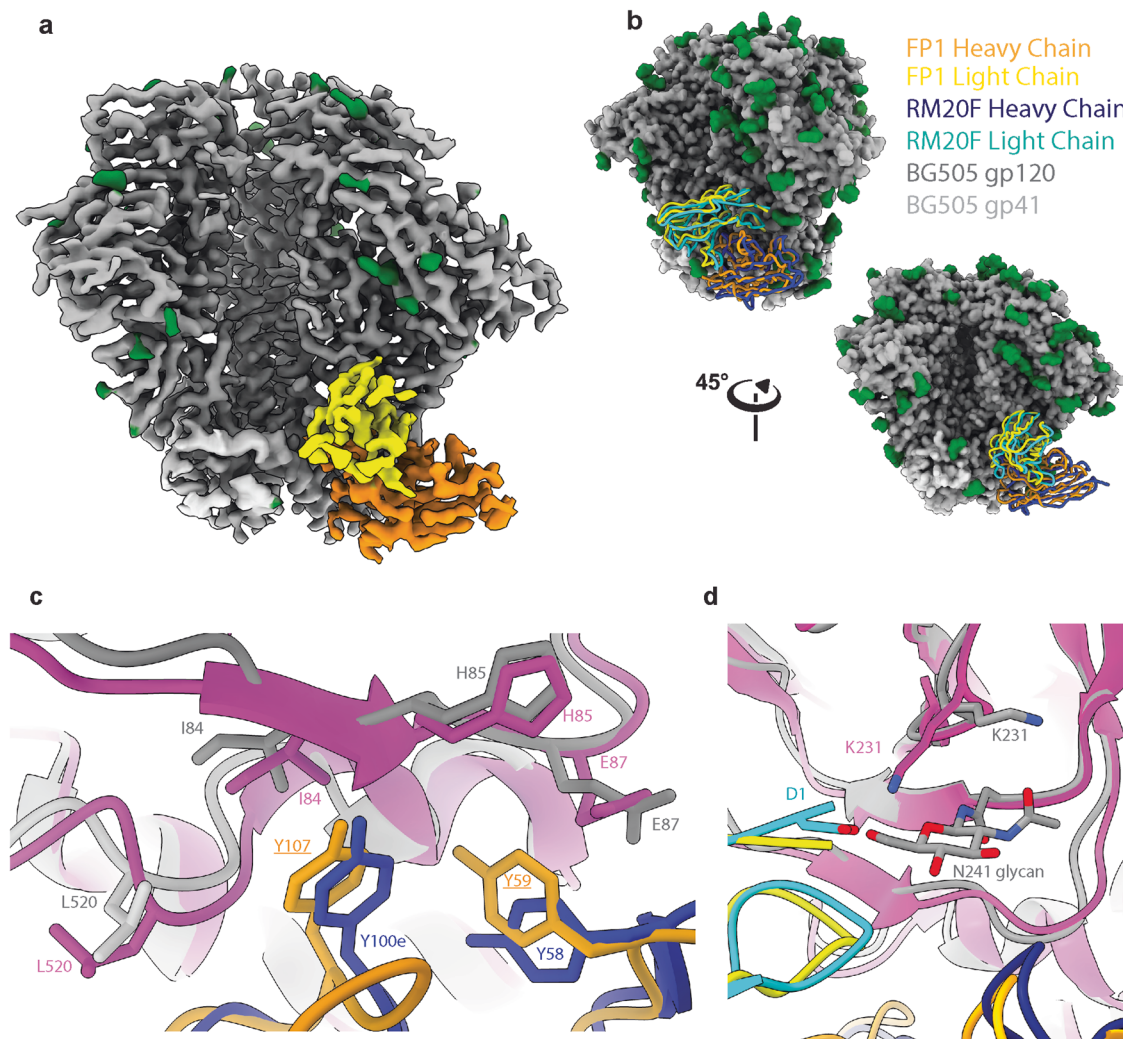
Fig. 6 | CryoEM Analysis of FP1. a Boost #2 in complex with predicted heavy chain (orange) and predicted light chain (yellow) of FP1. **b** Alignment of FP1 (orange and yellow) with RM20F (dark and light blue) with two views. **c** Both RM20F HCDR3 (dark blue) and FP1 predicted HCDR3 (orange) interact with I84 and H85 (grey for Boost #2 orientation for FP1 interactions; pink for BG505 residue orientation for RM20F (6VN0)) with a hydrophobic residue Y100e for RM20F and predicted Y106

(Y100c; Kabat) of FP1. HCDR2 of both FP1 and RM20F interact with H85 and E87 with hydrophobic residues at position 59 and 58, respectively. **d** N-terminus of RM20F (light blue) creates a salt-bridge with BG505 SOSIP.664 K231. This conformation of K231 is not allowed in the presence of the N241 glycan as in FP1 when complexed with BG505 Boost #2.

pumps were removed after 4 weeks and replaced with new pumps. At the conclusion of the sixth pump (week 24), the pumps were removed, and the animals received bilateral, bolus, s.c. immunizations with 59.6 μg (118 μg total dose) of an octameric nanoparticle[62,63] formulated in 30 μg 3M-052-squalene emulsion adjuvant (60 μg total dose) in each mid-thigh. At week 40, the animals received additional bilateral, bolus, s.c. immunizations with 50 μg (100 μg total dose) soluble Env trimer immunogen formulated in 375 μg (750 μg total dose) SMNP adjuvant[46] in each mid-thigh. Blood was collected at various time points into CPT tubes for PBMC and plasma isolation. Serum was isolated using serum collection tubes and frozen. Plasma was used in ELISA and EMPEM analysis. Serum was used for neutralization assays.

Lymph node fine needle aspirates and FACS
Prime-AviB and Boost#2-AviB were individually premixed with fluorochrome-conjugated streptavidin (SA-Alexa Fluor 647 [Ax647] or SA-Brilliant Violet 421 [BV421]) at RT for 20 minutes. LN FNAs were used to sample at both right and left inguinal LNs. Draining LNs were identified by palpitation and FNAs were performed by a veterinarian as described previously[15,47]. Fresh cells from the FNAs were incubated with probes for

30 minutes at 4 °C, washed twice with FACS buffer (PBS + 1% (v/v) Fetal bovine serum) and then incubated with surface antibodies (Table S5) for 30 minutes at 4 °C. Cells were washed twice more with FACS buffer and sorted on an FACSAria II. B cells were defined as live $CD20^+CD4^-CD8^-CD16^-$, non-IgM^+IgG^+ cells. B_{GC} cells were further defined as CD71+/CD38−B cells.

Monoclonal antibody production
Monoclonal IgGs were expressed in HEK293F cells and purified using affinity chromatography. Briefly, HEK293F cells (Invitrogen) were co-transfected with heavy and light chain plasmids (1:1 ratio) using PEImax. Transfections were performed according to the manufacturer's protocol. Supernatants were harvested 4-6 days following transfection and passed through a 0.45 μm filter. IgGs were purified using MAbSelect™ (GE Healthcare) affinity chromatography.

ELISAs
BG505 SOSIP IgG binding ELISA were conducted as described previously[64]. For the T33-31 ELISAs: Microlon half-area 96-well plates were coated overnight with 3 μg/mL T33-31 nanoparticle core protein in 0.1 M

NaHCO$_3$, pH 9. The plates were washed 3 times with wash buffer (TBS + 0.1% (v/v) Tween-20) and blocked overnight with PBS + 3% (w/v) BSA. The plates were washed 3 times with wash buffer and purified IgG from week 26 plasma was added in series for 5-fold dilutions starting at 1000 μg/mL in PBS + 1% (w/v) BSA. The plates were incubated at RT for 2 h and washed 3 times with wash buffer. Alkaline Phosphatase-conjugated AffiniPure Goat Anti-Human IgG/Fc secondary antibody (Jackson ImmunoResearch) was added at a 1:5000 dilution and allowed to bind for 1 h at RT. The plates were washed 4 times with wash buffer before being developed with 1-Step PNPP substrate (ThermoFisher) for ~30 minutes. Absorbance at 405 nm was recorded and data was analyzed with Prism version 8.4.2.

TZM-bl cell-based neutralization assays – BG505 and FP-sensitive panels

Serum neutralization assays were conducted using the single-round infection assay of TZM-bl cells with HIV-1 Env-pseudoviruses as described previously[65–71]. Neutralizing antibodies were measured as a function of reductions in luciferase (Luc) reporter gene expression after a single round of infection in TZM-bl cells[66,67]. TZM-bl cells (also called JC57BL-13) were obtained from the NIH AIDS Research and Reference Reagent Program, as contributed by John Kappes and Xiaoyun Wu. This is a HeLa cell clone that was engineered to express CD4 and CCR5[68] and to contain integrated reporter genes for firefly luciferase and E. coli beta-galactosidase under control of an HIV-1 LTR[69]. Briefly, a pre-titrated dose of virus was incubated with serial 3-fold dilutions of heat-inactivated (56 °C, 30 minutes) serum samples in duplicate in a total volume of 150 µl for 1 h at 37 °C in 96-well flat-bottom culture plates. Freshly trypsinized cells (10,000 cells in 100 µl of growth medium containing 75 µg/ml DEAE dextran) were added to each well. One set of control wells received cells + virus (virus control) and another set received cells only (background control). After 48 hours of incubation, 100 µl of cells was transferred to a 96-well black solid plate (Costar) for measurements of luminescence using the Britelite Luminescence Reporter Gene Assay System (PerkinElmer Life Sciences). Neutralization titers are the dilution of serum samples at which relative luminescence units (RLU) were reduced by 50% compared to virus control wells after subtraction of background RLUs. Assay stocks of molecularly cloned Env-pseudotyped viruses were prepared by transfection in 293 T/17 cells (American Type Culture Collection) and titrated in TZM-bl cells as described[66,67]. Mutations were introduced into Env plasmids by site-directed mutagenesis and confirmed by full-length Env sequencing by Sanger Sequencing, using Sequencher and SnapGene for sequence analyses. This assay has been formally optimized and validated[70] and was performed in compliance with Good Clinical Laboratory Practices, including participation in a formal proficiency testing program[71].

TZM-bl cell-based neutralization assays – global panel

Envelope pseudovirus production. Envelope pseudoviruses were generated through the cotransfection of the pSG3ΔEnv backbone plasmid (obtained from the NIH AIDS Research and Reference Reagent Program, Division of AIDS, NIAID, NIH)[69,72] and a plasmid encoding the full Env gp160 in a 3:1 ratio in HEK293T cells (ATCC) using the PEIMAX transfection reagent (Polysciences). Following 48 hours, the media was filtered through a 0.45 µm Steriflip unit (EMD Millipore), aliquoted, frozen and titrated. Mutations were introduced into Env plasmids by site-directed mutagenesis and confirmed by full-length Env sequencing by Sanger Sequencing, using Geneious Prime v8 for sequence analyses.

Neutralization assay. The neutralization assay[70] was performed with DMEM (Corning) supplemented with 10% FBS (Corning), 1% L-glutamine (Corning), 0.5% Gentamicin (Sigma), 2.5% HEPES (Gibco) and all incubations were performed at 37 °C, 5% CO2. On day one, 25 µL diluted pseudovirus mixed with 25 µL of 1:3 serially-diluted serum or control antibody was incubated for 1 hour, followed by the addition of 20 µL of TZM-bl cells at a concentration of 500, 000 cells/mL with DEAE-Dextran at a final concentration of 40 µg/mL. These were incubated for

24 hours and on day two, 130 µL of fresh DMEM was added and the samples which were once again incubated overnight. Finally, on day three the media was completely removed and 60 µL lysis buffer together with 60 µL luciferase substrate (Promega) was added per well, and luminescence was measured on the Synergy2 plate reader (BioTek). Neutralization data is reported as ID50 or IC50 (µg/mL) values which was calculated as the dilution or concentration at which a 50% reduction in infection was observed. Neutralization assays were performed in triplicate and SEM is reported. The TZM-bl cell line engineered from CXCR4-positive HeLa cells to express CD4, CCR5, and a firefly luciferase reporter gene (under control of the HIV-1 LTR) was obtained from the NIH AIDS Research and Reference Reagent Program, Division of AIDS, NIAID, NIH (developed by Dr. John C. Kappes, and Dr. Xiaoyun Wu).

Bio-Layer Interferometry (BLI)

An Octet RED instrument (FortéBio) was used to measure antibody–antigen interactions by Biolayer Interferometry. MAbs were loaded onto anti-human Fc (AHC) biosensors (FortéBio) at a concentration of 5 µg/mL in kinetics buffer (PBS, pH 7.4, 0.01% [w/v] BSA, and 0.002% [v/v] Tween 20) until a response of 1 nanometer shift was reached. Loaded biosensors were dipped into kinetics buffer for 1 min to acquire a baseline and then moved to wells containing the immunogens in kinetics buffer, at 1000 nM. The trimers were allowed to associate for 180 secs before the biosensor were moved back to the wells containing kinetics buffer where the baseline was acquired. Disassociation of the trimers from the IgG-loaded biosensors was recorded for 300 secs. All BLI experiments were conducted at 25 °C.

Electron Microscopy Polyclonal Epitope Mapping (EMPEM)

Plasma samples were heat-inactivated at 56 °C for 1 h. Polyclonal IgG was purified from plasma using Protein A resin (GE Healthcare) and digested into Fabs using immobilized papain resin as described previously[48]. Digested Fabs were passed over Protein A resin to remove Fc and undigested IgG. BG505 SOSIP/Fab complexes were made by mixing 10–15 µg SOSIP with 500 to 1000 µg of polyclonal Fabs. The mixture was allowed to incubate for 18 to 24 h at room temperature (RT). The complexes were SEC purified using a Superose™ 6 Increase 10/300 GL (GE Healthcare) column to remove excess Fab prior to EM grid preparation. Fractions containing the SOSIP/Fab complexes were pooled and concentrated using 10 kDa Amicon® spin concentrators (Millipore). Samples were diluted to ~0.03 mg/mL in TBS (0.05 M Tris pH 7.4, 0.15 M NaCl) and adsorbed onto glow discharged carbon-coated Cu400 EM grids (Electron Microscopy Sciences) and blotted after 10 seconds. The grids were then stained with 3 µL of 2% (w/v) uranyl formate, immediately blotted, and stained again for 45 secs followed by a final blot. Image collection and data processing was performed as described previously on a FEI Talos microscope (1.98 Å/pixel; 72,000 × magnification) with an electron dose of ~25 electrons/Å^2 using Leginon[73,74]. 2D classification, 3D sorting and 3D refinement conducted using Relion v3.0[75]. EM density maps were visualized using UCSF Chimera and segmented using Segger[76,77].

CryoEMPEM sample preparation

~7 mg of clean polyclonal fab from animal Rh.32613 at week 42 time point was complexed with 200 µg of BG505 SOSIP Boost 2 antigen. Sample was allowed to complex overnight (~18 hours) at room temperature and were SEC purified on a HiLoad 16/600 Superdex 200 pg column (GE Healthcare) using TBS as a running buffer. Sample was then concentrated to 6.1 mg/ml for application onto cryoEM grids.

CryoEMPEM-grid preparation and CryoEM imaging

Experiments were carried out as described previously[49]. We used a Vitrobot mark IV (Thermo Fisher Scientific) for cryo-grid preparation. Chamber temperature was set to 10 °C, maintained humidity at 100% with a varied blotting time within a range of 4.5–7.5 s, and blotting force was set to 0 with a wait time of 10 s. Prior to sample application, we combined the sample with lauryl maltose neopentyl glycol (LMNG) at a final concentration of

0.005 mM. We used UltrAuFoil R 1.2/1.3 (Au, 300-mesh; Quantifoil Micro Tools GmbH) grids for freezing. Grids were also treated with Ar/O$_2$ (Solaris plasma cleaner, Gatan) for 10 s. 3 μl of sample with LMNG were applied to the grid before being blot and then plunge-frozen into liquid-nitrogen-cooled liquid ethane. Grids were imaged using a K3 Summit direct electron detector camera (Gatan) that was mounted to an FEI Titan Krios electron microscope (Thermo Fisher Scientific) operating at 300 kV, which also had an autoloader. Images were collected at an exposure magnification of 97,000 resulting in pixel size at the specimen plane of 0.5155 Å.

CryoEMPEM – data processing
CryoEMPEM processing was performed similarly as described previously[49]. MotionCor2 was used for micrograph movie frame alignment and dose-weighting. Data processing was initially performed using cryoSPARCv2.15[78]. We used GCTF for CTF parameter estimation[79]. From cryoSPARC, trimer-fab complex particles were picked using template picker and run through two rounds of 2D classification to remove bad particle picks. From cryoSPARC, particles were transferred to Relion v3.0 to continue processing[75]. In relion, particles then underwent a third round of 2D classification followed by 3D refinement on selected particles. Next, we followed with a continue-refine job with a mask around the trimer only and then the map was postprocessed with the trimer-only mask. We performed a round of CTF refinement on these particles, which were then used as inputs for another round of 3D refinement. The resulting particle stack was then symmetry expanded for the next step, focused classification. A 40 Å sphere mask was appropriately placed in chimera around 6 epitopes: FP/N611, IF, V1V2V3, N355/N289, N618/N625 and the Base. We next generated trimer-Fab masks for each trimer-Fab maps resolved in the focused classification. Maps were postprocessed using the corresponding trimer-Fab mask. Two additional rounds of 3D classification were performed with tighter masks around the trimer-Fv (variable domain of the Fab). Maps were again postprocessed and then subjected to a CTF-refinement for each sorted class of particles. 3D refinement was repeated on particles after the CTF refinement step. Maps were postprocessed using a tight Trimer-Fv mask one final time to generate the high-resolution maps interpreted above (Supplementary Fig. 4).

CryoEMPEM – model building and refinement
Relion postprocessed maps were used for model building and refinement. The BG505 SOSIP structure from PDB entry 6V0R[27] was docked into each map using UCSF Chimera and was then mutated to match BG505 SOSIP Boost 2 used in this study. Polyalanine Fab models were also docked into each map. Heavy and light chains were assigned by comparing CDR3 lengths and the conformations of FR2 and FR3 between the H and L chains in the maps. CDR lengths were adjusted using manual model building in Coot[80,81] and the entire complex was refined in Rosetta[82] and Phenix[83,84]. For FP1 and FP3, each position in the heavy and light chain was mutated based on side chain density and assigned a confidence value as described in Antanasijevic et al.[58]. Briefly, each amino acid position was assigned a hierarchical category identifier which takes into consideration the degree of certainty and represents a predefined subset of amino acid residues that best correspond to the side chain density. The conserved disulfide pair of each chain and other IMGT anchor residues (i.e. W41) served as a fiducial markers. Sequences were then searched in a Juypter Notebook (www.jupyter.com) environment against the Indian origin rhesus macaque Germ Line Database (GLD)[26]. Individual scores were analyzed for FR1-3, and CDR1-2 to deduce the V_H and V_K/V_L gene usage of the predicted sequences. Top scoring sequences were analyzed with respect to the cryo-EM map, and the process was performed iteratively until convergence. Final models were evaluated using MolProbity[85] and EMRinger[86] and deposited to the PDB with polyclonal Fv regions modeled as polyalanine.

Data availability
Final cryo-EM models were deposition in the Protein Data Bank (PDB) under the following accession codes: 8SW7, 8T2E, 8SWW, 8SWV, 8SWX, and 8T2F, and the maps were also deposited in the Electron Microscopy Data Bank (EMDB) under the accession codes: EMD-40803 to EMD-40810, EMD-40822 to EMD-40824, and EMD-40981 and EMD-40982. Negative stain final reconstructions were deposited in the EMDB under the following accession codes: EMD-45102, EMD-45139 to EMD-45149.

References
1. National Center for Immunization and Respiratory Diseases. General recommendations on immunization – recommendations of the Advisory Committee on Immunization Practices (ACIP). *MMWR Recomm. Rep.* **60**, 1–64 (2011).
2. Watson, J. C. et al. An evaluation of measles revaccination among school-entry-aged children. *Pediatrics* **97**, 613–618 (1996).
3. Poland, G. A. et al. Measles reimmunization in children seronegative after initial immunization. *JAMA* **277**, 1156–1158 (1997).
4. Banatvala, J. E. & Van Damme, P. Hepatitis B vaccine do we need boosters? *J. Viral Hepat.* **10**, 1–6 (2003).
5. Miner, M. D., Corey, L. & Montefiori, D. Broadly neutralizing monoclonal antibodies for HIV prevention. *J. Int AIDS Soc.* **24**, e25829 (2021).
6. Corey, L. et al. Two randomized trials of neutralizing antibodies to prevent HIV-1 acquisition. *N. Engl. J. Med* **384**, 1003–1014 (2021).
7. Walker, B. D. The AMP Trials - A glass half full. *N. Engl. J. Med* **384**, 1068–1069 (2021).
8. Klein, F. et al. Somatic mutations of the immunoglobulin framework are generally required for broad and potent HIV-1 neutralization. *Cell* **153**, 126–138 (2013).
9. Kwong, P. D. & Mascola, J. R. Human antibodies that neutralize HIV-1: identification, structures, and B cell ontogenies. *Immunity* **37**, 412–425 (2012).
10. Andrabi, R. et al. Identification of common features in prototype broadly neutralizing antibodies to HIV envelope V2 Apex to facilitate vaccine design. *Immunity* **43**, 959–973 (2015).
11. Verkoczy, L., Kelsoe, G., Moody, M. A. & Haynes, B. F. Role of immune mechanisms in induction of HIV-1 broadly neutralizing antibodies. *Curr. Opin. Immunol.* **23**, 383–390 (2011).
12. Sather, D. N. et al. Factors associated with the development of cross-reactive neutralizing antibodies during human immunodeficiency virus type 1 infection. *J. Virol.* **83**, 757–769 (2009).
13. Burton, D. R. & Hangartner, L. Broadly neutralizing antibodies to HIV and their role in vaccine design. *Annu Rev. Immunol.* **34**, 635–659 (2016).
14. Kepler, T. B. et al. Immunoglobulin gene insertions and deletions in the affinity maturation of HIV-1 broadly reactive neutralizing antibodies. *Cell Host Microbe* **16**, 304–313 (2014).
15. Cirelli, K. M. et al. Slow delivery immunization enhances HIV neutralizing antibody and germinal center responses via modulation of immunodominance. *Cell* **177**, 1153–1171.e28 (2019).
16. Hu, J. K. et al. Murine antibody responses to cleaved soluble HIV-1 envelope trimers are highly restricted in specificity. *J. Virol.* **89**, 10383–10398 (2015).
17. Pauthner, M. et al. Elicitation of robust Tier 2 neutralizing antibody responses in nonhuman primates by HIV envelope trimer immunization using optimized approaches. *Immunity* **46**, 1073–1088.e6 (2017).
18. Tam, H. H. et al. Sustained antigen availability during germinal center initiation enhances antibody responses to vaccination. *Proc Natl Acad Sci USA.* **113**, E6639–E6648 (2016).
19. Binley, J. M. et al. Profiling the specificity of neutralizing antibodies in a large panel of plasmas from patients chronically infected with human immunodeficiency virus type 1 subtypes B and C. *J. Virol.* **82**, 11651–11668 (2008).
20. West, A. P. et al. Computational analysis of anti-HIV-1 antibody neutralization panel data to identify potential functional epitope residues. *Proc. Natl Acad. Sci. USA* **110**, 10598–10603 (2013).

21. Burton, D. R. et al. A blueprint for HIV vaccine discovery. *Cell Host Microbe* **12**, 396–407 (2012).

22. Hraber, P. et al. Prevalence of broadly neutralizing antibody responses during chronic HIV-1 infection. *AIDS* **28**, 163–169 (2014).

23. Kong, R. et al. Fusion peptide of HIV-1 as a site of vulnerability to neutralizing antibody. *Science* **352**, 828–833 (2016).

24. Cheng C., et al. Immune monitoring reveals fusion peptide priming to imprint cross-clade HIV-neutralizing responses with a characteristic early B cell signature. *Cell Rep.* **32**, 107981 (2020).

25. Van Gils, M. J. et al. An HIV-1 antibody from an elite neutralizer implicates the fusion peptide as a site of vulnerability. *Nat. Microbiol.* **2**, 16199 (2016).

26. Cottrell, C. A. et al. Mapping the immunogenic landscape of near-native HIV-1 envelope trimers in non-human primates. *PLoS Pathog.* **16**, e1008753 (2020).

27. Nogal, B. et al. Mapping polyclonal antibody responses in non-human primates vaccinated with HIV env trimer subunit vaccines. *Cell Rep.* **30**, 3755–3765.e7 (2020).

28. Lee, J. H. et al. Long-primed germinal centres with enduring affinity maturation and clonal migration. *Nature* **609**, 998–1004 (2022).

29. Kong, R. et al. Antibody lineages with vaccine-induced antigen-binding hotspots develop broad HIV neutralization. *Cell* **178**, 567–584.e19 (2019).

30. Xu, K. et al. Epitope-based vaccine design yields fusion peptide-directed antibodies that neutralize diverse strains of HIV-1. *Nat. Med.* **24**, 857–867 (2018).

31. Torrents de la Peña, A. et al. Improving the immunogenicity of native-like HIV-1 envelope trimers by hyperstabilization. *Cell Rep.* **20**, 1805–1817 (2017).

32. Wagh, K. et al. Completeness of HIV-1 envelope glycan shield at transmission determines neutralization breadth. *Cell Rep.* **25**, 893–908.e7 (2018).

33. McCoy, L. E. et al. Holes in the glycan shield of the native HIV envelope are a target of trimer-elicited neutralizing antibodies. *Cell Rep.* **16**, 2327–2338 (2016).

34. Klasse, P. J. et al. Sequential and simultaneous immunization of rabbits with HIV-1 envelope Glycoprotein SOSIP.664 trimers from Clades A, B and C. *PLoS Pathog.* **12**, e1005864 (2016).

35. Derking, R. et al. Enhancing glycan occupancy of soluble HIV-1 envelope trimers to mimic the native viral spike. *Cell Rep.* **35**, 108933 (2021).

36. Yang, Y. R. et al. Autologous antibody responses to an HIV envelope glycan hole are not easily broadened in rabbits. *J. Virol.* **94**, e01861–19 (2020).

37. Lee, J. H. et al. A broadly neutralizing antibody targets the dynamic HIV Envelope Trimer Apex via a long, rigidified, and anionic β-Hairpin structure. *Immunity* **46**, 690–702 (2017).

38. Walker, L. M. et al. Broad neutralization coverage of HIV by multiple highly potent antibodies. *Nature* **477**, 466–470 (2011).

39. Marasco, W. A. et al. Characterization of the cDNA of a broadly reactive neutralizing human anti-gp120 monoclonal antibody. *J. Clin. Invest* **90**, 1467–1478 (1992).

40. Blattner, C. et al. Structural delineation of a quaternary, cleavage-dependent epitope at the gp41-gp120 interface on intact HIV-1 Env trimers. *Immunity* **40**, 669–680 (2014).

41. Heath, P. T. et al. Safety and Efficacy of NVX-CoV2373 Covid-19 Vaccine. *N. Engl. J. Med* **385**, 1172–1183 (2021).

42. Lövgren Bengtsson, K., Morein, B. & Osterhaus, A. D. ISCOM technology-based Matrix M™ adjuvant: success in future vaccines relies on formulation. *Expert Rev. Vaccines* **10**, 401–403 (2011).

43. Hebeis, B. J. et al. Activation of virus-specific memory B cells in the absence of T cell help. *J. Exp. Med* **199**, 593–602 (2004).

44. Lutz, J. et al. Reactivation of IgG-switched memory B cells by BCR-intrinsic signal amplification promotes IgG antibody production. *Nat. Commun.* **6**, 8575 (2015).

45. Van Hoeven, N. et al. A formulated TLR7/8 agonist is a flexible, highly potent and effective adjuvant for pandemic influenza vaccines. *Sci. Rep.* **7**, 46426 (2017).

46. Silva, M. et al. A particulate saponin/TLR agonist vaccine adjuvant alters lymph flow and modulates adaptive immunity. *Sci. Immunol.* **6**, eabf1152 (2021).

47. Havenar-Daughton, C. et al. Direct probing of germinal center responses reveals immunological features and bottlenecks for neutralizing antibody responses to HIV Env Trimer. *Cell Rep.* **17**, 2195–2209 (2016).

48. Bianchi, M. et al. Electron-Microscopy-based epitope mapping defines specificities of polyclonal antibodies elicited during HIV-1 BG505 envelope trimer immunization. *Immunity* **49**, 288–300.e8 (2018).

49. Antanasijevic, A. et al. Polyclonal antibody responses to HIV Env immunogens resolved using cryoEM. *Nat. Commun.* **12**, 4817 (2021).

50. Havenar-Daughton, C., Lee, J. H. & Crotty, S. Tfh cells and HIV bnAbs, an immunodominance model of the HIV neutralizing antibody generation problem. *Immunol. Rev.* **275**, 49–61 (2017).

51. Nogal, B. et al. HIV envelope trimer-elicited autologous neutralizing antibodies bind a region overlapping the N332 glycan supersite. *Sci. Adv.* **6**, eaba0512 (2020).

52. Klasse, P. J. et al. Epitopes for neutralizing antibodies induced by HIV-1 envelope glycoprotein BG505 SOSIP trimers in rabbits and macaques. *PLoS Pathog.* **14**, e1006913 (2018).

53. deCamp, A. et al. Global panel of HIV-1 Env reference strains for standardized assessments of vaccine-elicited neutralizing antibodies. *J. Virol.* **88**, 2489–2507 (2014).

54. Lee, J. H., Ozorowski, G. & Ward, A. B. Cryo-EM structure of a native, fully glycosylated, cleaved HIV-1 envelope trimer. *Science* **351**, 1043–1048 (2016).

55. Yuan, M. et al. Conformational plasticity in the HIV-1 fusion peptide facilitates recognition by broadly neutralizing antibodies. *Cell Host Microbe* **25**, 873–883.e5 (2019).

56. Zheng, Z., Yang, R., Bodner, M. L. & Weliky, D. P. Conformational flexibility and strand arrangements of the membrane-associated HIV Fusion Peptide Trimer Probed By Solid-state NMR Spectroscopy. *Biochemistry* **45**, 12960–12975 (2006).

57. van Gils, M. J. & Sanders, R. W. Broadly neutralizing antibodies against HIV-1: Templates for a vaccine. *Virology* **435**, 46–56 (2013).

58. Antanasijevic, A. et al. From structure to sequence: Antibody discovery using cryoEM. *Sci. Adv.* **8**, eabk2039 (2022).

59. Pancera, M. et al. Structure and immune recognition of trimeric pre-fusion HIV-1 Env. *Nature* **514**, 455–461 (2014).

60. Kumar, S. et al. Capturing the inherent structural dynamics of the HIV-1 envelope glycoprotein fusion peptide. *Nat. Commun.* **10**, 763 (2019).

61. De Taeye, S. W. et al. Immunogenicity of stabilized HIV-1 envelope trimers with reduced exposure of non-neutralizing epitopes. *Cell* **163**, 1702–1715 (2015).

62. Bale, J. B. et al. Structure of a designed tetrahedral protein assembly variant engineered to have improved soluble expression. *Protein Sci.* **24**, 1695–1701 (2015).

63. Antanasijevic, A. et al. Structural and functional evaluation of de novo-designed, two-component nanoparticle carriers for HIV Env trimer immunogens. *PLoS Pathog.* **16**, e1008665 (2020).

64. Sok, D. et al. Recombinant HIV envelope trimer selects for quaternary-dependent antibodies targeting the trimer apex. *Proc. Natl Acad. Sci. USA* **111**, 17624–17629 (2014).

65. Seaman, M. S. et al. Tiered categorization of a diverse panel of HIV-1 Env Pseudoviruses for assessment of neutralizing antibodies. *J. Virol.* **84**, 1439–1452 (2010).

66. Montefiori, D. C. Measuring HIV neutralization in a Luciferase Reporter Gene Assay. *Methods Mol. Biol.* **485**, 395–405 (2009).

67. Li, M. et al. Human immunodeficiency virus type 1 env clones from acute and early subtype B infections for standardized assessments of vaccine-elicited neutralizing antibodies. *J. Virol.* **79**, 10108–10125 (2005).

68. Platt, E. J., Wehrly, K., Kuhmann, S. E., Chesebro, B. & Kabat, D. Effects of CCR5 and CD4 cell surface concentrations on infections by macrophagetropic isolates of human immunodeficiency virus type 1. *J. Virol.* **72**, 2855–2864 (1998).

69. Wei, X. et al. Emergence of resistant human immunodeficiency virus type 1 in patients receiving fusion inhibitor (T-20) monotherapy. *Antimicrob. Agents Chemother.* **46**, 1896–1905 (2002).

70. Sarzotti-Kelsoe, M. et al. Optimization and validation of the TZM-bl assay for standardized assessments of neutralizing antibodies against HIV-1. *J. Immunol. Methods* **409**, 131–146 (2014).

71. Todd, C. A. et al. Development and implementation of an international proficiency testing program for a neutralizing antibody assay for HIV-1 in TZM-bl cells. *J. Immunol. Methods* **375**, 57–67 (2012).

72. Wei, X. et al. Antibody neutralization and escape by HIV-1. *Nature* **422**, 307–312 (2003).

73. Pugach, P. et al. A Native-Like SOSIP.664 trimer based on an HIV-1 subtype B env Gene. *J. Virol.* **89**, 3380–3395 (2015).

74. Suloway, C. et al. Automated molecular microscopy: the new Leginon system. *J. Struct. Biol.* **151**, 41–60 (2005).

75. Zivanov, J. et al. New tools for automated high-resolution cryo-EM structure determination in RELION-3. *Elife* **7**, e42166 (2018).

76. Pettersen, E. F. et al. UCSF Chimera–a visualization system for exploratory research and analysis. *J. Comput Chem.* **25**, 1605–1612 (2004).

77. Pintilie, G. D., Zhang, J., Goddard, T. D., Chiu, W. & Gossard, D. C. Quantitative analysis of cryo-EM density map segmentation by watershed and scale-space filtering, and fitting of structures by alignment to regions. *J. Struct. Biol.* **170**, 427–438 (2010).

78. Punjani, A., Rubinstein, J. L., Fleet, D. J. & Brubaker, M. A. cryoSPARC: algorithms for rapid unsupervised cryo-EM structure determination. *Nat. Methods* **14**, 290–296 (2017).

79. Zhang, K. Gctf: Real-time CTF determination and correction. *J. Struct. Biol.* **193**, 1–12 (2016).

80. Emsley, P. & Crispin, M. Structural analysis of glycoproteins: building N-linked glycans with Coot. *Acta Crystallogr D. Struct. Biol.* **74**, 256–263 (2018).

81. Emsley, P., Lohkamp, B., Scott, W. G. & Cowtan, K. Features and development of Coot. *Acta Crystallogr D. Biol. Crystallogr* **66**, 486–501 (2010).

82. Wang, R. Y. R. et al. Automated structure refinement of macromolecular assemblies from cryo-EM maps using Rosetta. *Elife* **5**, e17219 (2016).

83. Liebschner, D. et al. Macromolecular structure determination using X-rays neutrons and electrons: recent developments in Phenix. *Acta Crystallogr. Sec. D Struct. Biol.* **75**, 861–877 (2019).

84. Afonine, P. V. et al. Real-space refinement in PHENIX for cryo-EM and crystallography. *Acta Crystallogr. Sec. D Struct. Biol.* **74**, 531–544 (2018).

85. Williams, C. J. et al. MolProbity: More and better reference data for improved all-atom structure validation. *Protein Sci.* **27**, 293–315 (2018).

86. Barad, B. A. et al. EMRinger: side chain-directed model and map validation for 3D cryo-electron microscopy. *Nat. Methods* **12**, 943–946 (2015).

Acknowledgements

Author contributions

C.A.C. – Conceptualization, Data curation, Formal Analysis, Investigation, Methodology, Validation, Visualization, Writing - original draft, Writing – review & editing. P.P.P. – Data curation, Formal Analysis, Investigation, Visualization, Writing – original draft, Writing – review & editing. K.M.C. – Formal Analysis, Investigation, Visualization, Writing – review and editing. D.G.C. – Resources. C.A.E. – Resources, A.A. – Formal Analysis, Investigation, Methodology, Software. G.O. – Formal Analysis, Investigation, Methodology, Software, Visualization, Writing – review & editing. L.M.S. – Investigation, H.G. – Investigation, Resources, J.D.A. – Formal Analysis, Investigation, Visualization. B.N. – Investigation, M.S. – Investigation, J.B. – Investigation, M.P., Writing – review and editing – Investigation, D.J.I. – Resources, D.M. – Resources, Max Crispin – Resources, D.R.B. – Funding acquisition, Supervision. G.S. – Resources, S.C. – Conceptualization, Funding Acquisition, Project Administration, Supervision, Writing – review and editing. A.B.W. – Conceptualization, Funding acquisition, Project Administration, Supervision, Writing – review and editing. C.A.C. and P.P.P. are co-authors on this manuscript.

Competing interests

The authors declare no competing interests.

Additional information

Supplementary information The online version contains supplementary material available at https://doi.org/10.1038/s41541-024-00918-9.

Correspondence and requests for materials should be addressed to Andrew B. Ward.

Reprints and permissions information is available at http://www.nature.com/reprints

Publisher's note Springer Nature remains neutral with regard to jurisdictional claims in published maps and institutional affiliations.